RSC Advances

PAPER

View Article Online
View Journal | View Issue

Cite this: *RSC Adv.*, 2022, **12**, 28678

Defect-rich graphene-coated metamaterial device for pesticide sensing in rice†

Wendao Xu,[abc] Qi Wang,[abc] Ruiyun Zhou,[abc] Saima Hameed,[abc] Yungui Ma,[d] Lijuan Xie[abc] and Yibin Ying*[abc]

Received 23rd September 2022
Accepted 30th September 2022

DOI: 10.1039/d2ra06006j

rsc.li/rsc-advances

Performing sensitive and selective detection in a mixture is challenging for terahertz (THz) sensors. In light of this, many methods have been developed to detect molecules in complex samples using THz technology. Here we demonstrate a defect-rich monolayer graphene-coated metamaterial operating in the THz regime for pesticide sensing in a mixture through strong local interactions between graphene and external molecules. The monolayer graphene induces a 50% change in the resonant peak excited by the metamaterial absorber that could be easily distinguished by THz imaging. We experimentally show that the Fermi level of the graphene can be tuned by the addition of molecules, which agrees well with our simulation results. Taking chlorpyrifos methyl in the lixivium of rice as a sample, we further show the molecular sensing potential of this device, regardless of whether the target is in a mixture or not.

1. Introduction

Graphene, owing to its unique electrical and optical properties,[1,2] has been utilized in diverse fields including sources,[3,4] detectors,[5] modulators,[6] and sensors[7,8] covering a wide spectral range. Graphene based optical modulators working in the visible/near infrared (NIR),[9] mid-infrared (MIR),[10] and terahertz (THz) band[11] show tunable properties with external electrical and/or optical stimuli. To ensure tunable properties of these devices, a graphene layer needs to be carefully transferred onto a flat surface for its electrical continuation, which requires high quality chemical vapor deposition (CVD)-grown graphene as well as experienced graphene transferring skills. Therefore, constructing tunable graphene devices no longer limited by electrical continuation requirements is meaningful for an easy fabrication route and of great interest to diverse research fields.

It is well known that THz wave is the last part of the electromagnetic wave to be explored. Since the absorption of THz wave is dominated by the excitation of intramolecular and intermolecular vibrations,[12] some chemicals such as drugs,[13,14] pesticide,[15] and carbohydrate[16] show fingerprint absorption peaks in THz band. To enhance the interaction between molecule and THz wave, the localized resonances excited by metamaterials which show an intense enhanced electromagnetic field near the metallic structures are utilized.[17–19] However, THz metamaterial lakes in sensing selectivity[20] which limits its practical applications in detecting hazard molecules in a mixture. Taking advantage of the great biomolecular affinity *via* π-electrons, graphene has been utilized in chemical analyte detection,[21] aptamer sensing,[22] and fluorescence transducing.[23] By integrating metamaterials and graphene, the hybrid graphene metamaterial device shows sensing[8,24] and modulating[11] applications, indicating that graphene is a promising material in potential practical applications in THz regime.

Here we fabricate a defect-rich monolayer graphene-coated metamaterial operating in THz regime for pesticide sensing in a mixture. We select THz waveband as our target frequency band not only it is rich with spectral fingerprints[16,25] but also defects occur more frequently in THz devices comparing to visible/NIR or MIR devices because of the longer wavelength. We present an experimental demonstration of a THz graphene-coated metamaterial reaching an intensity of modulation depth up to 14% when the lixivium of unhusked rice contaminated by chlorpyrifos methyl molecules is coated on its surface, which indicates that the chemical doping method of graphene still works for this defect-rich graphene-coated metamaterial despite those cracks in the monolayer graphene layer. Our research shows that analytes with π-electrons like chlorpyrifos methyl with the concentration of 2.5 mg L^{-1} in the lixivium of rice can interact with graphene through π–π stacking,[26] holding the feasibility of molecular sensing, even in a complex mixture. Currently, few work on analyte detection in a mixture using metamaterials has been reported.[27] Using metamaterials only is

[a]College of Biosystems Engineering and Food Science, Zhejiang University, 866 Yuhangtang Rd., 310058 Hangzhou, P.R. China. E-mail: yingyb@zju.edu.cn

[b]Key Laboratory of Intelligent Equipment and Robotics for Agriculture of Zhejiang Province, P.R. China

[c]Key Laboratory of on Site Processing Equipment for Agricultural Products, Ministry of Agriculture and Rural Affairs, P.R. China

[d]State Key Laboratory for Modern Optical Instrumentation, College of Optical Science and Engineering, Zhejiang University, 866 Yuhangtang Rd., 310058 Hangzhou, P.R. China

† Electronic supplementary information (ESI) available. See DOI: https://doi.org/10.1039/d2ra06006j

hard to discriminate abundant types of sensing targets as metamaterials responded to the refractive index of sample, remaining a challenge for the applications in selective sensing. Therefore, our work provides an effective and simple method to fabricate graphene-coated metamaterials beyond the limitation of electrical continuation requirement for chemical doping and sensing purpose. This method could also be utilized in diverse potential practical application cases.

2. Experimental section

2.1. Equipments

A THz time-domain spectrometer system (Z-3, Zomega Corporation, East Greenbush, NY, USA) was used to measure the broadband reflection spectra and image with a spectral range of 0.1–3.5 THz. The imaging area of the metamaterial device was 9 mm*3 mm. THz system was purged with nitrogen to prevent THz absorption from water vapor (the humidity was less than 1%) and the temperature was 23 ± 1 °C. The signal-to-noise ratio (SNR) was over 40 dB for all the THz spectral measurements.

2.2. Fabrication of graphene-coated THz metamaterial device

CVD grown monolayer graphene (Trivial Transfer Graphene, TTG) was purchased from ACS Material (Medford, MA, USA). It was released onto water for at least two hours and then transferred onto the surface of metamaterial device. By removing the polymethyl methacrylate (PMMA) on the top of graphene using acetone,[28] a defect-rich monolayer graphene-coated THz metamaterial device was obtained for future tests.

2.3. Sample preparation and THz measurements

Chlorpyrifos methyl (>98%) was purchased from Aladdin Corporation (China). The original lixivium of husked/unhusked rice was obtained by adding 10 mL deionized water to 5 g husked/unhusked rice and let it stand still for half an hour. The original lixivium of husked/unhusked rice contaminated by chlorpyrifos methyl was obtained by adding 10 mL solution with a concentration of chlorpyrifos methyl set as 2.5 mg L^{-1} to 5 g husked/unhusked rice and let it stand still for half an hour. The original lixivium was diluted to 4%, 8%, 24%, 40%, and 100% for future tests; accordingly, the concentration of chlorpyrifos methyl in the lixivium were 0.1, 0.2, 0.6, 1.0, and 2.5 mg L^{-1}. Before adding lixivium sample, monolayer graphene-coated metamaterials were clearly washed thrice with deionized water. In this work, 10 μL of desired lixivium was dropped on the surface of monolayer graphene-coated THz metamaterials with three duplicates. Then the sample was dried at room temperature before THz measurements. Each spectrum was averaged by four scans.

3. Results and discussion

3.1. Fabrication and characteristics of graphene-coated THz metamaterial

In this work, the metamaterial structure we used consists of an aluminum ground plane and a planar array of square patch gold resonators which are spaced by a thin polyimide film (ESI†).[29] This metal–dielectric-metal tri-layer structure leads to significant field enhancement and near unity absorption at its resonant frequency.[30–32] By transferring monolayer graphene onto the metamaterial, monolayer graphene-coated THz metamaterial is obtained (Fig. 1a). The photograph and the scanning electron microscope (SEM) image of monolayer graphene-coated THz metamaterial are shown in Fig. 1b and c.

We further investigate the defect condition of graphene-coated THz metamaterial. As presented in Fig. 1d and e, the cracks can be easily observed at the boundaries of gold patch. In contrast, the SEM image of the metamaterial without graphene shows a surface without any cracks (Fig. 1f). We attribute those cracks to the height mismatch between the graphene layer and gold patch. As presented in Fig. 1g, one dimensional height profile of gold patch resonator boundary shows a 450 nm height difference, which is much too larger than the thickness of graphene (~0.3 nm). Comparing to tunable graphene devices that required strictly electrical continuation, our graphene devices are no longer limited by this condition as the sensing performance is enabled by chemical doping of external molecules. Thereby, the fabrication route is much simpler with less failure in device preparation. We also note that the monolayer graphene can be transferred onto the surface of silicon[33] and quartz.[34] The graphene monolayer is confirmed by Raman spectroscopy with a high-intensity 2D peak (~2680 cm^{-1}) and a low-intensity G peak (~1580 cm^{-1}) (Fig. 1h).

3.2. THz imaging properties of THz metamaterial with/without graphene

To investigate THz properties of graphene-coated metamaterial device, we measured imaging properties as well as spectral changes induced by monolayer graphene covering the metamaterial (Fig. 2a). The optical image of THz metamaterial device (Fig. 2b) accords well with THz image of metamaterial device with/without graphene at 0.85 THz (Fig. 2c). As revealed by THz reflection spectrum of metamaterial device with/without graphene in Fig. 2d, the addition of the monolayer graphene results in an obvious increase of the metamaterial reflection. The reflectance is approximately 10% at 0.87 THz for the metamaterial structure with gold patch length 95 μm, presenting a strong resonant absorption. Here the reflectance is defined as $R = |E_{sample}/E_{reference}|^2$ where E_{sample} ($E_{reference}$) is the intensity of THz electric field collected from the graphene metamaterial sample (silver mirror). Note that the transmission of this device is 0 because the back-reflector (aluminum) prevents all THz wave from passing through this graphene THz metamaterial. This intense resonant peak has already shown its ability in sensing applications in the literature.[35,36] The reflectance of graphene-coated metamaterial reaches 60% at resonant peak,

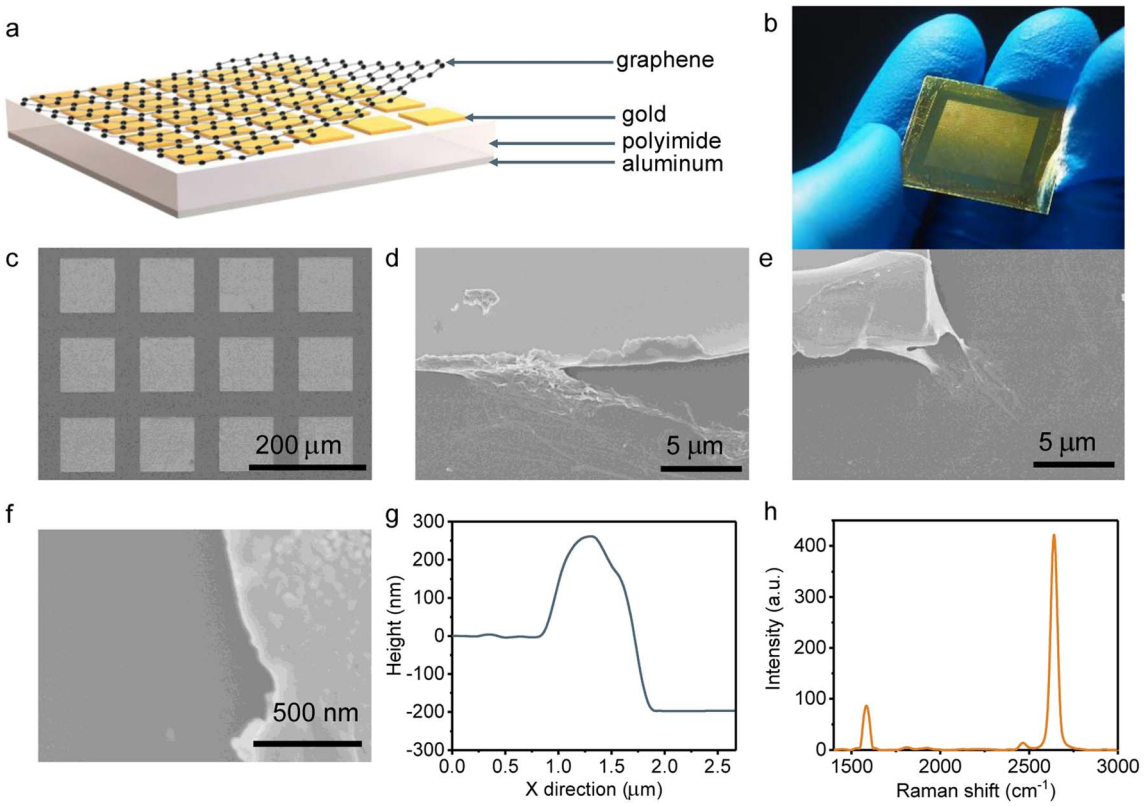

Fig. 1 Monolayer graphene-coated THz metamaterial device. (a) Schematic of monolayer graphene-coated THz metamaterials. (b) Photograph of the graphene-coated THz metamaterials. (c) SEM image of graphene-coated THz metamaterials. (d and e) SEM image of the surface of metamaterials, showing the cracks of transferred graphene. (f) SEM image of the surface of metamaterial absorber without graphene layer. (g) One dimensional height profile of a graphene-coated THz metamaterial at the boundary of a gold patch resonator. (h) Raman spectroscopy of monolayer graphene-coated metamaterial.

indicating that the monolayer graphene induces 50% change of the reflectance, which accords well with the literature.[37] We also note the red shift of resonance frequency and decrease of quality factor (Q) can be observed, which agrees with the reported work.[38] As a kind of semimetal, graphene induces changes in impedance match situation of the metamaterial

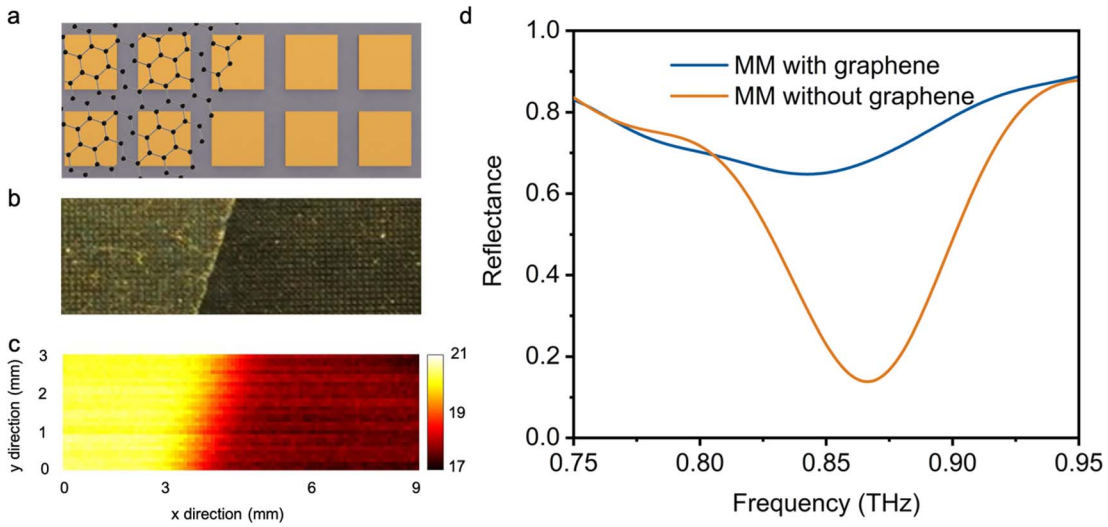

Fig. 2 THz imaging of monolayer graphene-coated THz metamaterial device. (a) Schematic of THz imaging area, including THz metamaterial with/without graphene. (b) Photograph of THz metamaterial device, the area is according to (a). (c) THz imaging of metamaterial device with/without graphene at 0.85 THz. day, THz reflection spectrum of metamaterial device with/without graphene.

absorber, which modifies dispersion of the top patch resonator arrays. Thereby, the monolayer graphene with a thickness less than 1 nm causes vast change from the metamaterial absorber which outweighs most dielectric materials.[39]

3.3. Sensing properties of graphene THz metamaterial

Chlorpyrifos methyl, as a member of broad-spectrum organophosphorous pesticides, has been world widely utilized for decades.[40] The monolayer graphene-coated metamaterial device with rich defects is utilized for sensing purpose by detecting chlorpyrifos methyl molecules in rice lixivium. The reflection spectra of graphene metamaterial in detecting rice lixivium contaminated by different concentrations of chlorpyrifos methyl ranging from 0.1 mg L^{-1} to 1.0 mg L^{-1} is shown in Fig. 3a. With the existence of analyte, a higher Q factor can be clearly observed comparing to the graphene coated metamaterial alone, which is different from the reported work showing a decreased Q factor during sensing process.[41] The observed sensing property of graphene-coated metamaterial is induced by the unique interaction between external molecules and the graphene-coated metamaterial. External molecules interact with graphene at its close vicinity through delocalized π-electrons,[42] which moves the Fermi level toward the Dirac point and as a result, the carrier density in graphene is reduced.[43,44] The interaction of external molecules and Dirac electrons affects the doping level of graphene.[45,46] Therefore, the conductivity decreases and the resonance of metamaterial enhances, resulting in a consecutive Q factor improvement of resonant peak. With the concentration increase of chlorpyrifos methyl, the value of resonant peak decreases from 65% to 53%. We observe that at the concentration range of chlorpyrifos methyl from 0.1 mg L^{-1} to 1.0 mg L^{-1}, the interaction between external molecules and graphene does exist as the resonant peak increases.

The sensing mechanism is further validated utilizing FDTD numerical simulations and a reflective mode from a monolayer graphene-coated metamaterial with Fermi level varying from 20 meV to 120 meV below the Dirac point is shown in Fig. 3b. The resonant reflectance of graphene-coated metamaterial is higher than that of metamaterial without graphene on its surface, which accords well with the data presented in Fig. 2d. This damped resonant peak is caused by the modification of metamaterial absorber cavity induced by monolayer graphene. The resonant reflectance of monolayer graphene-coated metamaterial decreases when the Fermi level shifted toward the Dirac point, thereby, an increased Q factor can be observed.

3.4. Detection of chlorpyrifos methyl molecules on unhusked rice

As reported in the literature,[43,44] molecule has a benzene like ring structure with π-electrons can strongly interact with graphene through π–π stacking. In contrast, other molecules without π-electrons in their molecule structure have a much weaker interaction with graphene, presenting a lower sensitivity comparing to molecules containing π-electrons.[24] Therefore, graphene-coated metamaterial holds the feasibility in sensing molecules containing π-electrons in a complex mixture. Our work elucidates this point by detecting chlorpyrifos methyl molecules in the lixivium of rice as the pesticide molecule has π-electrons and the main content of the lixivium of rice, starch, does not have π-electrons. The schematic figure of the reflective sensing using monolayer graphene-coated THz metamaterial is illustrated in Fig. 4a. The molecule structure of chlorpyrifos methyl which contains a benzene like ring structure with π-electrons is also demonstrated in Fig. 4b.

When the lixivium of unhusked rice contaminated by chlorpyrifos methyl solution is dropped and dried on the surface of graphene-metamaterial device, the relative reflectance changes (Fig. 4c), which is defined as $\Delta R/R=(R_{reference}-R_{sample})/R_{reference}$, where R_{sample} ($R_{reference}$) is the reflectance at the resonant dip with (without) sensing targets. The value $\Delta R/R$ increases rapidly at low concentration (from 0.1 mg L^{-1} to 0.6 mg L^{-1}), and it continues to increase with a much slower rate. The value $\Delta R/R$ presents an inverse trend comparing to low

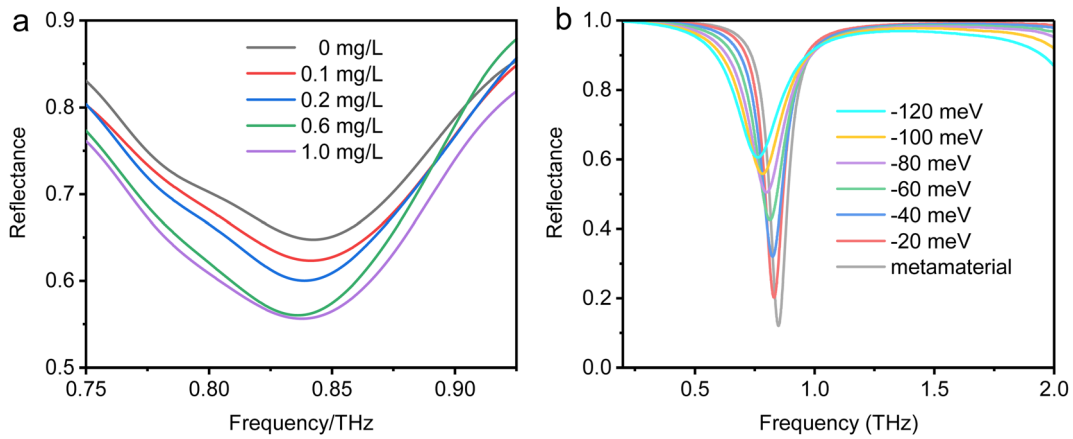

Fig. 3 Sensing properties of graphene THz metamaterials. (a) Experimentally measured reflection spectra of graphene metamaterial absorber with different concentration of chlorpyrifos methyl varying from 0.1 mg L^{-1} to 1.0 mg L^{-1}. (b) Numerically simulated reflection spectra of graphene-coated metamaterial absorbers with Fermi level ranging from 20 meV to 120 meV below the Dirac point.

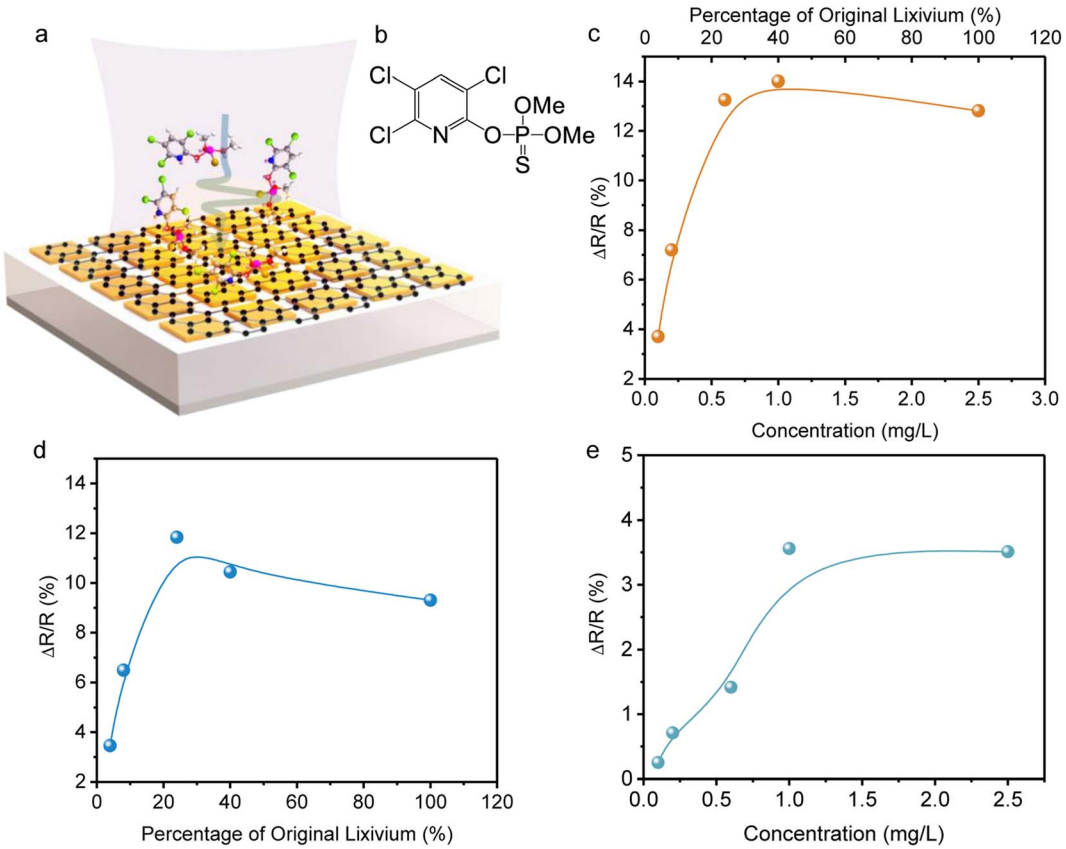

Fig. 4 Detection of chlorpyrifos methyl molecules on unhusked rice using monolayer graphene-coated THz metamaterial absorber. (a) Schematic of the sensing using monolayer graphene-coated THz metamaterial absorber. (b) Structure of a chlorpyrifos methyl molecule. (c) Relative reflectance changes of graphene-metamaterial absorber with the lixivium of unhusked rice and chlorpyrifos methyl solution coated on its surface. (d) Relative reflectance changes of graphene-metamaterial absorber with the lixivium of unhusked rice coated on its surface. (e) Relative differential reflectance changes when lixivium of unhusked rice with chlorpyrifos methyl molecules are coated on the surface of graphene-metamaterial heterostructure.

concentration cases at the concentration of 2.5 mg L^{-1}. As we discussed above, the increase of $\Delta R/R$ is induced by the interaction between graphene and external molecules which shifts the Fermi level of graphene toward Dirac point. With the increase of more external molecules, the interaction between additional part of external molecules and graphene becomes weaker than that between external molecules and the electric field excited by graphene-coated metamaterial, resulting in a red shift and decrease of Q factor of resonant dip.

Fig. 4d shows the relative reflectance changes of graphene-metamaterial device with the lixivium of unhusked rice coated on its surface. We can observe the same trend that the value $\Delta R/R$ increases rapidly at low percentage of original lixivium (from 3.5% to 12%), and then it decreases when the percentage of original lixivium further increases. We note that, comparing to the data plotted in Fig. 4c, the value $\Delta R/R$ of graphene-metamaterial (12%) with the lixivium of unhusked rice coated on its surface in Fig. 4d is smaller than that in Fig. 4c (14%). We attribute this to starch contains no π-electrons in its molecule structure and as a main content of this lixivium, it interacts with graphene in a weaker extent than molecules containing π-electrons such as chlorpyrifos methyl. Therefore, the maximal value $\Delta R/R$ of graphene-metamaterial with the lixivium of unhusked rice contaminated by chlorpyrifos methyl solution outweighs that of lixivium of unhusked rice only.

Relative differential reflectance changes of lixivium of unhusked rice with chlorpyrifos methyl molecules are presented in Fig. 4e, of which the data is derived from Fig. 4c and d. The value $\Delta R/R$ is induced by the addition of chlorpyrifos methyl molecules, showing a same trend as revealed in Fig. 4c and d. In this work, the chlorpyrifos methyl molecules in lixivium of unhusked rice induces a maximal $\Delta R/R$ value 3.5% at the concentration of 1.0 mg L^{-1} and the pesticide can be detected based on three times of signal to noise ratio, which meet the requirement of the World Health Organization's provisional guideline limit (1.0 mg L^{-1}).[47] Therefore, the graphene-coated metamaterial structure presents strong light matter interactions and enables sensitive detection of analyte layer on its top.

3.5. Detection of chlorpyrifos methyl molecules on husked rice

In contrast, we also performed the detection of chlorpyrifos methyl molecules on husked rice using monolayer graphene-

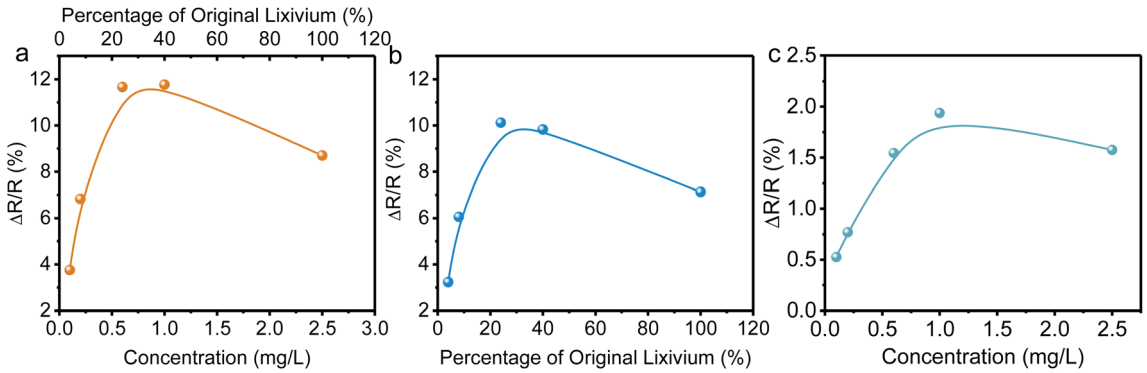

Fig. 5 Detection of chlorpyrifos methyl molecules on husked rice using monolayer graphene-coated THz metamaterial absorber. (a) Relative reflectance changes of graphene-metamaterial absorber with the lixivium of husked rice and chlorpyrifos methyl solution coated on its surface. (b) Relative reflectance changes of graphene-metamaterial absorber with the lixivium of husked rice coated on its surface. (c) Relative differential reflectance changes when lixivium of husked rice with chlorpyrifos methyl molecules are coated on the surface of graphene-metamaterial heterostructure.

coated THz metamaterial device. The relative reflectance changes of graphene-coated metamaterial with the lixivium of husked rice contaminated by chlorpyrifos methyl molecules coated on its surface is shown in Fig. 5a. The value $\Delta R/R$ increases rapidly at low concentration (from 0.1 mg L^{-1} to 0.6 mg L^{-1}), and it starts to decrease when the concentration further increases. The maximal value $\Delta R/R$ (11.5%) is smaller than that of the lixivium of unhusked rice contaminated by chlorpyrifos methyl molecules in Fig. 4c (here 14.0%), showing that the content of chlorpyrifos methyl molecules in the lixivium of husked rice is less than that in the lixivium of unhusked rice. Fig. 5b shows the relative reflectance changes of graphene-coated metamaterial with the lixivium of husked rice coated on its surface, presenting a same trend shown in Fig. 4d. Note that the maximal value $\Delta R/R$ induced by the lixivium of husked rice (10.0%) is also smaller than that of the lixivium of unhusked rice (12.0%), which indicates the content of chlorpyrifos methyl molecules in the lixivium of husked rice is less than that in the lixivium of unhusked rice.

We further calculate the relative differential reflectance changes of lixivium of husked rice with chlorpyrifos methyl molecules on the surface of graphene-coated metamaterial device, as presented in Fig. 5c. The original data is obtained from Fig. 5a and b. With the increase of chlorpyrifos methyl concentration, the value $\Delta R/R$ increases and reaches a maximal value 2.0%, which is smaller than the maximal $\Delta R/R$ in Fig. 4e when detecting chlorpyrifos methyl molecules in the lixivium of unhusked rice. This may attribute to the stronger adsorption of chlorpyrifos methyl molecules by husked rice than by unhusked rice.

4. Conclusion

Graphene and metamaterials have attracted tremendous attention due to their specific properties, unique physics and promising feasibility in modulation and sensing applications. Graphene based devices without the need to meet electrical continuation requirement will attract broad interest in diverse fields and further commercialization. In this work, we present a tunable defect-rich monolayer graphene-coated metamaterial operating in THz regime for chemical doping and sensing purposes. We found that external molecules can change the resonant magnitude by shifting the Fermi level of graphene, resulting an increase of Q value. Taking advantage that analytes with π-electrons can strongly interact with graphene through π–π stacking, we performed the detection of chlorpyrifos methyl (containing π-electrons) molecules in the lixivium of unhusked/husked rice, showing the molecular sensing potential of this device, regardless of whether the target is in the mixture or not. Our work provides an effective method to chemical dope graphene-coated metamaterials which is no longer limited by electrical continuation requirements, presenting the potential in accelerating a host of new modulation and sensing applications in the future.

Conflicts of interest

The authors declare no competing financial interest.

Acknowledgements

The authors gratefully acknowledge the financial support provided by the National Natural Science Foundation of China (Grant no. 32001413).

References

1 H. Yoo, R. Engelke, S. Carr, S. Fang, K. Zhang, P. Cazeaux, S. H. Sung, R. Hovden, A. W. Tsen, T. Taniguchi, K. Watanabe, G. Yi, M. Kim, M. Luskin, E. B. Tadmor, E. Kaxiras and P. Kim, *Nat. Mater.*, 2019, **18**, 448–453.
2 A. Kerelsky, L. J. Mcgilly, D. M. Kennes, L. Xian, M. Yankowitz, S. Chen, K. Watanabe, T. Taniguchi, J. Hone, C. Dean, A. Rubio and A. N. Pasupathy, *Nature*, 2019, **572**, 95–100.

3 R. Shiue, Y. Gao, C. Tan, C. Peng, J. Zheng, D. K. Efetov, Y. D. Kim, J. Hone and D. Englund, *Nat. Commun.*, 2019, **10**, 109.
4 H. Cong, F. Yang, C. Xue, K. Yu, L. Zhou, N. Wang, B. Cheng and Q. Wang, *Small*, 2018, **1704414**, 1–5.
5 E. O. Polat, G. Mercier, I. Nikitskiy, E. Puma, T. Galan, S. Gupta, M. Montagut, J. J. Piqueras, M. Bouwens, T. Durduran, G. Konstantatos, S. Goossens and F. Koppens, *Sci. Adv.*, 2019, **5**, 7846.
6 M. Said Ergoktas, S. Soleymani, N. Kakenov, K. Wang, T. B. Smith, G. Bakan, S. Balci, A. Principi, K. S. Novoselov, S. K. Ozdemir and C. Kocabas, *Science*, 2022, **376**, 184–188.
7 H. Hu, X. Yang, X. Guo, K. Khaliji, S. R. Biswas, F. J. G. De Abajo, T. Low, Z. Sun and Q. Dai, *Nat. Commun.*, 2019, **10**, 1131.
8 S. Lee, J. Choe, M. Seo, C. Kim, S. Bae, J. Kim and Q. Park, *Sens. Actuators, B*, 2020, **310**, 127841.
9 E. O. Polat and C. Kocabas, *Nano Lett.*, 2013, **13**, 5851–5857.
10 B. Zeng, Z. Huang, A. Singh, Y. Yao, A. K. Azad, A. D. Mohite, A. J. Taylor, D. R. Smith and H.-T. Chen, *Light: Sci. Appl.*, 2018, **7**, 51.
11 X. Chen, Z. Tian, Y. Lu, Y. Xu, X. Zhang, C. Ouyang, J. Gu, J. Han and W. Zhang, *Adv. Opt. Mater.*, 2020, **8**, 1900660.
12 B. Ferguson and X.-C. Zhang, *Nat. Mater.*, 2002, **1**, 26–33.
13 M. Tonouchi, *Nat. Photonics*, 2007, **1**, 97–105.
14 H. Lindley-Hatcher, J. Wang, A. I. Hernandez-Serrano, J. Hardwicke, G. Nurumbetov, D. M. Haddleton and E. Pickwell-MacPherson, *Pharmaceutics*, 2021, **13**, 2052.
15 R. Yang, Y. Li, B. Qin, D. Zhao, Y. Gan and J. Zheng, *RSC Adv.*, 2022, **12**, 1769–1776.
16 R. Damari, O. Weinberg, D. Krotkov, N. Demina, K. Akulov, A. Golombek, T. Schwartz and S. Fleischer, *Nat. Commun.*, 2019, **10**, 3248.
17 A. Ahmadivand, B. Gerislioglu, R. Ahuja and Y. K. Mishra, *Mater. Today*, 2020, **32**, 108–130.
18 N. H. Anh, M. Q. Doan, N. X. Dinh, T. Q. Huy, D. Q. Tri, L. T. Ngoc Loan, B. van Hao and A. T. Le, *RSC Adv.*, 2022, **12**, 10950–10988.
19 K. Yang, W. Yu, G. Huang, J. Zhou, X. Yang and W. Fu, *RSC Adv.*, 2020, **10**, 26824–26833.
20 W. Xu, S. Wang, W. Li, Z. Zhang, Y. Wang, Y. Yang, H. Zhang, P. Liu, L. Xie and Y. Ying, *Biosens. Bioelectron.*, 2022, **209**, 114274.
21 L. Tang, H. Feng, J. Cheng and J. Li, *Chem. Commun.*, 2010, **46**, 5882–5884.
22 X. Chen, Y. Liu, X. Fang, Z. Li, H. Pu, J. Chang, J. Chen and S. Mao, *Biosens. Bioelectron.*, 2019, **126**, 664–671.
23 M. T. Hwang, Z. Wang, J. Ping, D. K. Ban, Z. C. Shiah, L. Antonschmidt, J. Lee, Y. Liu, A. G. Karkisaval, A. T. C. Johnson, C. Fan, G. Glinsky and R. Lal, *Adv. Mater.*, 2018, **1802440**, 1–9.
24 W. Xu, L. Xie, J. Zhu, L. Tang, R. Singh, C. Wang, Y. Ma, H.-T. Chen and Y. Ying, *Carbon*, 2019, **141**, 247–252.
25 Y. Wang, X. Zhang, X. Zhang, T. Zhou, Z. Cui and K. Zhang, *J. Mater. Chem. A*, 2022, **10**, 1780–1787.
26 M. Sun and J. Li, *Nano Today*, 2018, **20**, 121–137.
27 D. Lee, G. Kim, C. Kim, Y. M. Jhon, S. Member, J. H. Kim, T. Lee, J. Son and M. Seo, *IEEE Trans. Terahertz Sci. Technol.*, 2016, **6**, 389–395.
28 A. Pirkle, J. Chan, A. Venugopal, D. Hinojos, C. W. Magnuson, S. McDonnell, L. Colombo, E. M. Vogel, R. S. Ruoff and R. M. Wallace, *Appl. Phys. Lett.*, 2011, **99**, 122108.
29 J. Zhu, Z. Ma, W. Sun, F. Ding, Q. He, L. Zhou and Y. Ma, *Appl. Phys. Lett.*, 2014, **105**, 021102.
30 L. Cong, S. Tan, R. Yahiaoui, F. Yan, W. Zhang and R. Singh, *Appl. Phys. Lett.*, 2015, **106**, 031107.
31 H.-T. Chen, *Opt. Express*, 2012, **20**, 7165–7172.
32 N. I. Landy, S. Sajuyigbe, J. J. Mock, D. R. Smith and W. J. Padilla, *Phys. Rev. Lett.*, 2008, **100**, 207402.
33 L. Xu, J. Xu, W. Liu, D. Lin, J. Lei, B. Zhou, Y. Shen and X. Deng, *Sens. Actuators, B*, 2022, **367**, 132016.
34 R. Zhou, C. Wang, Y. Huang, K. Huang, Y. Wang, W. Xu, L. Xie and Y. Ying, *Biosens. Bioelectron.*, 2021, **188**, 113336.
35 X. Yan, M. Yang, Z. Zhang, L. Liang, D. Wei, M. Wang, M. Zhang, T. Wang, L. Liu, J. Xie and J. Yao, *Biosens. Bioelectron.*, 2019, **126**, 485–492.
36 K. Yang, J. Li, M. Lamy de la Chapelle, G. Huang, Y. Wang, J. Zhang, D. Xu, J. Yao, X. Yang and W. Fu, *Biosens. Bioelectron.*, 2021, **175**, 112874.
37 W. Gao, J. Shu, K. Reichel, D. v. Nickel, X. He, G. Shi, R. Vajtai, P. M. Ajayan, J. Kono, D. M. Mittleman and Q. Xu, *Nano Lett.*, 2014, **14**, 1242–1248.
38 F. Valmorra, G. Scalari, C. Maissen, W. Fu, C. Schönenberger, J. W. Choi, H. G. Park, M. Beck and J. Faist, *Nano Lett.*, 2013, **13**, 3193–3198.
39 W. Xu, L. Xie, J. Zhu, X. Xu, Z. Ye, C. Wang, Y. Ma and Y. Ying, *ACS Photonics*, 2016, **3**, 2308–2314.
40 F. S. Rodriguez, P. R. Armstrong, E. B. Maghirang, K. F. Yaptenco, E. D. Scully, F. H. Arthur, D. L. Brabec, A. D. Adviento-Borbe and D. C. Suministrado, *Appl. Eng. Agric.*, 2020, **36**, 983–993.
41 R. Singh, W. Cao, I. Al-Naib, L. Cong, W. Withayachumnankul and W. Zhang, *Appl. Phys. Lett.*, 2014, **105**, 171101.
42 F. Schedin, A. Geim, S. Morozov, E. Hill, P. Blake, M. Katsnelson and K. Novoselov, *Nat. Mater.*, 2007, **6**, 652–655.
43 Y. Guo, Y. Han, Y. Guo and C. Dong, *Biosens. Bioelectron.*, 2013, **45**, 95–101.
44 F. Ortmann, W. G. Schmidt and F. Bechstedt, *Phys. Rev. Lett.*, 2005, **95**, 186101.
45 K. S. Novoselov, A. K. Geim, S. V Morozov, D. Jiang, M. I. Katsnelson, I. V Grigorieva, S. V Dubonos and A. A. Firsov, *Nature*, 2005, **438**, 197–200.
46 A. Ashraf, Y. Wu, M. C. Wang, K. Yong, T. Sun, Y. Jing, R. T. Haasch, N. R. Aluru and S. Nam, *Nano Lett.*, 2016, **16**, 4708–4712.
47 W. Xu, L. Xie, J. Zhu, W. Wang, Z. Ye, Y. Ma, C. Y. Tsai, S. Chen and Y. Ying, *Food Chem.*, 2017, **218**, 330–334.